Letter

Dynamical phase transitions of information flow in random quantum circuits

J.-Z. Zhuang,[1,*] Y.-K. Wu,[1,2] and L.-M. Duan[1,2,†]

[1]*Center for Quantum Information, Institute for Interdisciplinary Information Sciences, Tsinghua University, Beijing 100084, People's Republic of China*

[2]*Hefei National Laboratory, Hefei 230088, People's Republic of China*

(Received 15 April 2023; revised 7 August 2023; accepted 4 December 2023; published 26 December 2023)

We study how the information flows in many-body dynamics governed by random quantum circuits and discover a rich set of dynamical phase transitions in this information flow. The phase-transition points and their critical exponents are established across Clifford and Haar random circuits through finite-size scaling. The flow of both classical and quantum information, measured respectively by Holevo and coherent information, shows similar dynamical phase transition behaviors. We investigate how the phase transitions depend on the initial location of the information and the final probe region, and find ubiquitous behaviors in these transitions, revealing interesting properties about the information propagation and scrambling in this quantum many-body model. Our paper underscores rich behaviors of the information flow in large systems with numerous phase transitions, thereby sheds light on the understanding of quantum many-body dynamics.

DOI: 10.1103/PhysRevResearch.5.L042043

Introduction. Information flow in a quantum many-body system usually accompanies the growth of quantum entanglement and drives the system toward thermalization [1]. Apart from being essential in understanding nonequilibrium many-body physics, quantum dynamics about the information flow is also closely related to black hole theory and quantum gravity through the AdS/CFT correspondence [2,3]. Under short-range interactions, the propagation of information is limited in a light-cone structure governed by the Lieb-Robinson bound [4,5]. On the other hand, in the long-time limit, quantum information scrambling [6,7] will occur for generic chaotic quantum systems, such that information initially encoded in localized degrees of freedom will spread over the whole system and cannot be recovered by local operations [5,8,9]. However, the detailed process between these two extreme cases is less well understood and involves rich phenomena like prethermalization [10], many-body localization [11,12], and many-body scars [13,14].

Here we study the information retrievable from a subsystem of an initially locally encoded system, whose temporal derivative manifests the information flow. We adopt the random quantum circuit ansatz as depicted in Fig. 1(a), which is widely used to capture universal quantum dynamics in a chaotic system without being exposed to the detailed Hamiltonian [15–19]. By considering the information flow as a function of system parameters, we uncover a spectrum of behaviors beyond the light-cone and scrambling dynamics. Specifically, the information flow undergoes sudden shifts and can be used to delineate phase boundaries as a function of time and other system parameters. Similar to how order parameters switch from zero to nonzero values across a phase boundary, it exhibits distinct behaviors as the ratio of evolution time t to the system size N goes across the critical points in the thermodynamic limit $N \to \infty$, thereby exhibiting dynamical phase transitions (DPTs). Note that there are various notions of DPT in the literatures [20]. The most widely used definition is based on the nonanalytical behavior of the Loschmidt echo in closed many-body systems under Hamiltonian evolution [21,22], which is deeply connected to conventional partition functions. However, this definition has no direct counterpart in random unitary circuits. On the other hand, DPT is defined differently in open quantum many-body systems [23,24] and under the scenario of computational complexity [25].

Our key observation is the existence of dynamical phase transitions and their universality across both classical and quantum information, as well as within Clifford and Haar random circuits. We study their physical meanings by quantifying the DPTs' positions and critical exponents using finite-size scaling. We study primarily the Clifford random circuits for the convenience of large-scale numerical simulation [26–28], and generalization is verified for generic quantum circuit ansatz [29,30]. We also provide a general picture of information propagation that applies to generic random circuit model setups. The discovery of such rich phase transition behavior sheds light on the understanding of quantum many-body dynamics.

Dynamical phase transitions in information flow. Consider an N-qubit quantum system with periodic boundary condition, as shown in Fig. 1(a). We consecutively select S qubits as the source of information $\mathcal{S}$ and M qubits as the measurement subsystem $\mathcal{M}$. We encode information into $\mathcal{S}$, apply a random circuit U, trace out the complement of $\mathcal{M}$ as the environment $\mathcal{E}$, and retrieve the information from $\mathcal{M}$.

*zhuangjz21@mails.tsinghua.edu.cn
†lmduan@tsinghua.edu.cn

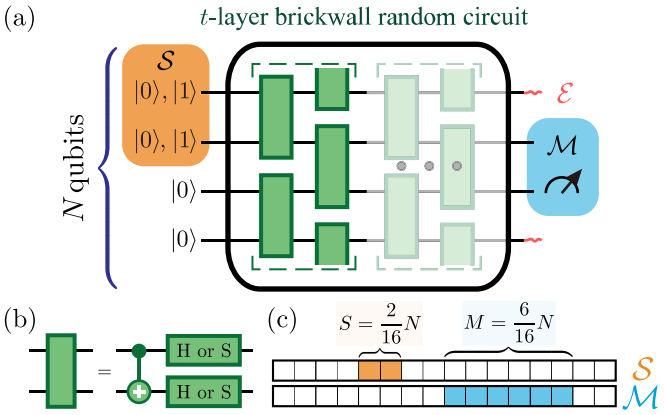

FIG. 1. Model for probing information dynamics. (a) Information is encoded into an S-qubit source in an N-qubit system with periodic boundary condition. Then after t layers of brick-wall-structured random circuits, we trace out the environment and retrieve the information from the remaining M-qubit measurement subsystem. Each "brick" (green rectangle) represents a random operation between the two nearby qubits. Here $N = 4$ for illustration. (b) In each two-qubit random operation, we first apply a CNOT gate. Then independently for each qubit, we randomly apply a Hadamard or phase gate $\mathrm{diag}(1, e^{i\pi/2})$ with equal probability. (c) An example of source and measurement subsystem. For ease of expression, they are consecutively selected according to the 16 equal segments of the system.

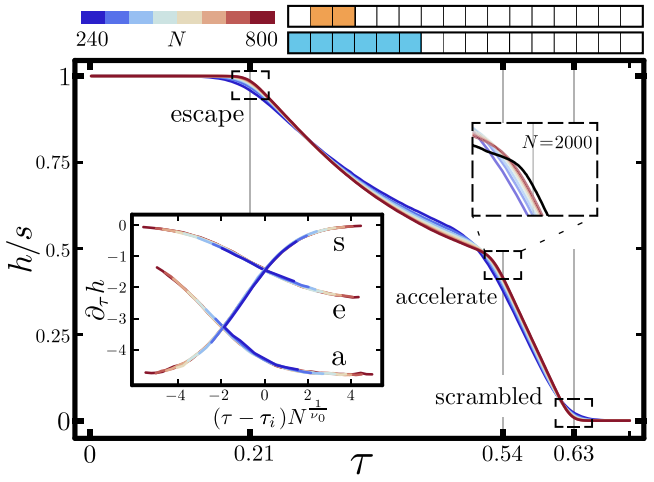

FIG. 2. Time evolution of average normalized Holevo information $h(\tau)$ under eight system sizes from $N = 240$ (blue) to $N = 800$ (red). We fix $s \equiv \frac{S}{N} = \frac{2}{16}$ and the measurement subsystem $m \equiv \frac{M}{N} = \frac{6}{16}$. At the three DPT points,the curve becomes sharp as N grows. We denote them from left to right as the τ_e, τ_a, and τ_s point. For the τ_a point, we show an additional curve to illustrate its position. The inset further demonstrates the transition by finite-size scaling of $\partial_\tau h$. We find the critical exponent $\nu_0 = 1.25$ and scale the τ axis near each of the three DPT points in the same way $\tau_i'(\tau) = (\tau - \tau_i)N^{\frac{1}{\nu_0}}$ where $i \in \{e, a, s\}$. All of the eight curves collapse. Each data point in the inset is obtained from over 6×10^4 samples.

We first study the classical information dynamics in the quantum system, and the quantum information will be discussed later. We encode S bits by preparing each qubit in $\mathcal{S}$ into $|0\rangle$ or $|1\rangle$ with equal probability. The rest of the qubits are initialized as $|0\rangle^{\otimes N-S}$. We denote the set of all the 2^S possible initial states as $\{|\psi_i\rangle\}_{i=1}^{2^S}$. After the random circuit, the extractable information can be quantified by the Holevo information

$$H(U) = S_{vn}\left(\sum_i p_i \rho_i^{\mathcal{M}}\right) - \sum_i p_i S_{vn}\left(\rho_i^{\mathcal{M}}\right) \qquad (1)$$

where $p_i = \frac{1}{2^S}$, $\rho_i^{\mathcal{M}} = \mathrm{Tr}_{\mathcal{E}}(U|\psi_i\rangle\langle\psi_i|U^\dagger)$ is the density matrix of $U|\psi_i\rangle$ in $\mathcal{M}$, S_{vn} denotes the von Neumann entropy.

The random circuit comprises t brick-wall layers, each corresponding to a unit of abstract time. Despite of stretched time scale, the structure of information dynamics is uniform across different probability distributions of the "bricks" over the Clifford group (see the Supplemental Material, SM [31]). As illustrated in Fig. 1(b), we set each brick as a CNOT gate followed by random single-qubit Clifford gates. We denote $\mathcal{U}_t$ as the set of all possible t-layered unitaries constructed in this way.

With fixed $s = \frac{S}{N}$ and $m = \frac{M}{N}$, we study our system under increasing system sizes N. We numerically calculate the time evolution of average Holevo information $H(t) = \frac{1}{|\mathcal{U}_t|}\sum_{U\in\mathcal{U}_t} H(U)$ and normalize it by $h(t) = \frac{H(t)}{N}$. The averaged value $h(t)$ is sufficient to characterize each $h(U)$ for generic $U \in \mathcal{U}_t$ because, as we show in the SM [31], its variance over $\mathcal{U}_t$ vanishes in the large N limit. We also normalize the time by $\tau = \frac{t}{N}$.

As a representative example, we place a $\frac{2N}{16}$-qubit source inside a $\frac{6N}{16}$-qubit measurement subsystem. The information dynamics $h(\tau)$ is shown in Fig. 2. In the limit of large N, three sharp turns of the curve can be observed, indicating discontinuous $\partial_\tau h$ around the three points. Further verification that they are DPT points and their physical meanings will be discussed later. We denote them by their τ-axis position τ_e (escape), τ_a (accelerate), and τ_s (scrambled). At early times $\tau < \tau_e$, $h(\tau)$ keeps its initial value s because the light-cones starting from $\mathcal{S}$ are still inside $\mathcal{M}$; at τ_e, information starts to decrease by escaping through the left boundary of $\mathcal{M}$. When $\tau = \tau_a$, the rate of decreasing accelerates; after $\tau > \tau_s$, the system becomes scrambled $h(\tau) = 0$, consistent with its infinite-time limit [32].

To further verify and analyze the critical behavior, we perform finite-size scaling near each of the three DPT points τ_i, $i \in \{e, a, s\}$. The curves $\partial_\tau h$ of different system sizes N collapse when we scale the τ axis by the form $\tau_i'(\tau) = (\tau - \tau_i)N^{\frac{1}{\nu_0}}$ where we find the critical exponent ν_0 to be equal for all i, as shown in the inset of Fig. 2. Thus, around each τ_i, we can express $\partial_\tau h$ of various N as a same function of τ_i'. Then taking the thermodynamic limit $N \to \infty$, we verify the nonanalyticity of information dynamics $\partial_\tau h(\tau_i - 0) \neq \partial_\tau h(\tau_i + 0)$. As will be discussed later, the critical exponent ν_0 is universal across various model configurations.

DPTs' positions and physical implications. In order to determine the physical meanings of the three DPT points, we study how their positions can be determined by the selection of $\mathcal{S}$ and $\mathcal{M}$. We begin by determining the τ-axis positions of the escape point τ_e and the scrambled point τ_s, before discussing the accelerate point τ_a.

With fixed s and m, we move $\mathcal{S}$ from the middle to the boundary of $\mathcal{M}$, as shown in Fig. 3(a). By the periodic bound-

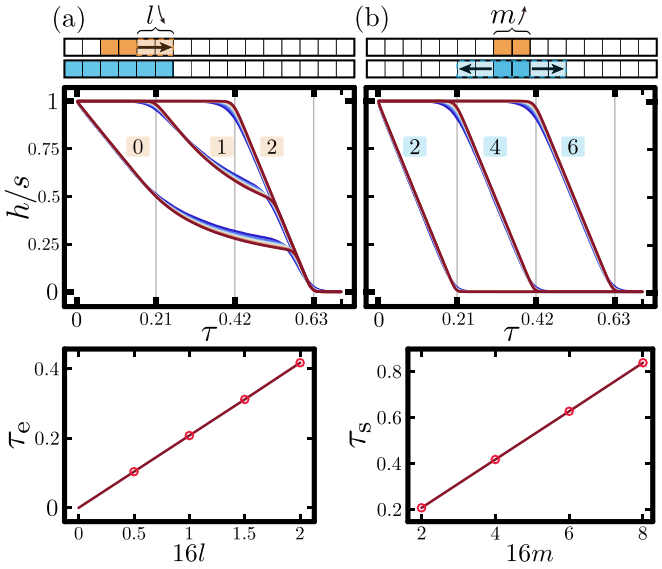

FIG. 3. Dynamics of $h(\tau)$ under different selections of the source $\mathcal{S}$ and the measurement subsystem $\mathcal{M}$. (a) We change the relative position between $\mathcal{S}$ and $\mathcal{M}$. We keep $\mathcal{S}$ inside $\mathcal{M}$ and fix $s = \frac{2}{16}$, $m = \frac{6}{16}$. Each group of curves is from various system sizes and labeled by the corresponding relative position $16l$, where l is the normalized distance between the right boundaries of $\mathcal{S}$ and $\mathcal{M}$. The escape point's position τ_e is proportional to l. The scrambled point τ_s stays invariant. (b) We change $\frac{2}{16} \leqslant m \leqslant \frac{1}{2}$ and fix $\mathcal{S}$ in the middle of $\mathcal{M}$. Each group of curves is labeled by $16m$. τ_s is proportional to m. For clarity, only part of the calculated $h(\tau)$ curves are shown.

ary condition, this only changes the relative position of $\mathcal{S}$ and $\mathcal{M}$. We define the normalized distance $l = \frac{L}{N}$ where L is the minimal distance from the qubits in $\mathcal{S}$ to the boundaries of $\mathcal{M}$. When l decreases, τ_e decreases linearly. When $l = 0$, the information can escape from $\mathcal{M}$ at the first circuit layer, and the τ_e point disappears at $\tau = 0$ as expected. We have $\tau_e(l) = l/v_e$. The scrambled point τ_s, which marks the transition from $h > 0$ to $h = 0$, is independent of l. Such independence holds for any arbitrary selection of $\mathcal{S}$ (see the SM [31]), as long as $h(\tau)$ is not exponentially so that τ_s does not vanish.

The scrambled point's position varies when m changes, as shown in Fig. 3(b) where we keep $\mathcal{S}$ fixed within $\mathcal{M}$. For $m < \frac{1}{2}$, we observe a linear dependence $\tau_s(m) = \frac{m}{2}/v_s$. Combined with invariant τ_s for arbitrary selections of $\mathcal{S}$, this implies that no information can be retrieved from any consecutive subsystem equal to or smaller than m after τ_s. Nonconsecutively selected subsystems of size m are also scrambled. One can see them scrambling faster by rearranging the qubits to make them consecutive and the resulting circuit would contain longer-range gates. We note that $\boldsymbol{v_s}$ can be directly connected with the entanglement velocity v_E [30], as demonstrated by the saturation of the entanglement entropy of $\mathcal{M}$ to its maximum value at τ_s.

We further found $v_s = v_e \equiv v_I$, which we denote as the information velocity. The above analysis can be summarized as

$$\begin{aligned} \tau_e(l) &= l/v_I \\ \tau_s(m) &= m/2v_I \end{aligned}, \tag{2}$$

which suggests a light-cone structure of information propagation underpinning both the τ_e and τ_s points. τ_e is the moment when light-cones emitted from the qubits in $\mathcal{S}$ reach the boundary of $\mathcal{M}$. Depending on whether they are exiting or entering $\mathcal{M}$, information starts to either decrease or increase. On the other hand, τ_s is the moment when $\mathcal{M}$ is entangled with M qubits, reflected by the light-cones emitted from $\mathcal{M}$ covering $2v_I t_s$ qubits outside of $\mathcal{M}$. To help understand the scrambling condition $\frac{M}{M+2v_I t_s} \leqslant \frac{1}{2}$, we note that this condition also applies when regarding the total $M + 2v_I t_s$ qubits as a maximally entangled system [32]. Such picture is also applicable both when $m > \frac{1}{2}$ and under the open boundary condition (see the SM [31]).

Although successful in predicting τ_e and τ_s, the light-cone picture cannot help understand the accelerate point τ_a. Specifically, the τ_a point is not "the time when light-cones start escaping from both ends of $\mathcal{M}$". For $l = 0$ ($l = \frac{1}{16}$) in Fig. 3(a), information can only reach the left boundary of $\mathcal{M}$ at $\tau = \frac{4}{16}/v_I$ ($\tau = \frac{3}{16}/v_I$), later than the actual τ_a. We further show that τ_a has a nonlinear dependence on the model's length-scale (see the SM [31]), suggesting that all linear light-cone understandings are insufficient. Also, the accelerate point still exists when $\mathcal{S}$ has no abrupt boundaries (see the SM [31]).

We have discussed above only $m < \frac{1}{2}$. For $m > \frac{1}{2}$, the τ_e and τ_s points still exist and are dominated by v_I. A major difference is that the τ_a point does not exist and, after τ_s, there are nontrivial dynamics followed by another DPT, which we denote as τ_r (recover). h reaches minimum at τ_s and saturates to its nonzero infinite-time limit through τ_r points. More details can be found in the SM [31].

Dynamics of quantum information. Coherent information quantifies the reliably transmitted qubits through a noisy quantum channel. In quantum communication, it characterizes the quantum channel capacity when the encoding scheme is optimal [33,34]. In quantum error correction, it upper bounds the number of qubits that can be recovered [35]. Using coherent information as a quantum counterpart of the Holevo information, we compare classical and quantum information dynamics.

We now study the quantum information flow with similar encoding scheme to that for the classical information. The only difference is that the initial state of the source would be an ensemble $\rho^{\mathcal{S}} = (\frac{1}{2}I)^{\otimes S}$. This is equivalent to mixing the pure states $\{|\psi_i\rangle\}_{i=1}^{2^S}$ in the classical information model. Applying random circuit U and tracing out the environment $\mathcal{E}$ form a quantum channel. The resulting coherent information $C^{\mathcal{M}}$ can be calculated as [35,36]

$$C^{\mathcal{M}} = S_{vn}(\rho^{\mathcal{M}}) - S_{vn}(\rho^{\mathcal{E}}) \tag{3}$$

where $\rho^{\mathcal{M}} = \mathrm{Tr}_{\mathcal{E}}(U(\rho^{\mathcal{S}} \otimes |0\rangle\langle 0|^{\otimes N-S})U^\dagger)$ is the density matrix of $\mathcal{M}$, and $\rho^{\mathcal{E}}$ is similarly defined by exchanging $\mathcal{E}$ and $\mathcal{M}$.

Like what we have done to the Holevo information, we average the coherent information over $\mathcal{U}_t$ and define $c = \frac{C^{\mathcal{M}}}{N}$. We calculate $c(\tau)$ for various positions of $\mathcal{S}$ and $\mathcal{M}$ with their sizes s and m fixed.

As shown in Fig. 4(a), when $\mathcal{S}$ is inside (outside) of $\mathcal{M}$, c is initialized at its upper (lower) bound, indicating that all of the information are contained in $\mathcal{M}$ (lost into $\mathcal{E}$). The escape point's position $\tau_e(l) = l/v_I$ is the same as that in the classical information model, verifying its physical meaning. For $\mathcal{S}$

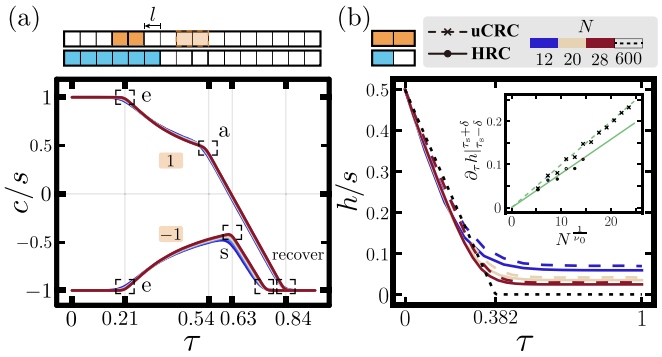

FIG. 4. Universality of DPT points in quantum circuit ansatz. (a) Dynamics of average normalized coherent information $c(\tau)$. We again specify $s = \frac{2}{16}$ and $m = \frac{6}{16}$. $\mathcal{S}$ is inside (outside) of $\mathcal{M}$ with the boundary distance $l = 1$ (denoted as $l = -1$). For $l = 1$, up to three DPT points τ_e, τ_a, and τ_r can be observed. Additionally, c crosses from positive to negative at τ_s. For $l = -1$, the τ_a point does not exist and a DPT at τ_s appears. (b) Information dynamics in Haar random circuits (HRC, solid line) and uniform sampling Clifford random circuits (uCRC, dashed line). Here, we set the system size from $N = 12$ (blue) to $N = 28$ (red) and fix $s = 1, m = \frac{1}{2}$. $h(\tau)$ in both systems exhibit similar behavior. The inset shows the scaling behavior of $\partial_\tau h|_{\tau_s-\delta}^{\tau_s+\delta} \propto N^{\frac{1}{\nu_0}}$ under both HRC and uCRC where the same critical exponent $\nu_0 = 1.25$ is applied. τ_s is from the thermodynamic limit of uCRC and $\delta = 0.012$ is a constant.

inside $\mathcal{M}$, c turns from positive to negative at τ_s, indicating that the amount of remaining quantum information turns to none. This is in agreement with the DPT point τ_s in classical information dynamics. c converges to its infinite-time limit $-s$ through the last DPT. Consistent with the classical model for $m > \frac{1}{2}$, we denote it as the τ_r point.

We can understand the above phenomena in the context of private classical information transmission [36–38]. We encode classical information by $\{|\psi_i\rangle\}_{i=1}^{2^S}$ and give a penalty of -1 whenever one bit of information is leaked to and recoverable from the environment. The result $C^{\mathcal{M}} = H^{\mathcal{M}} - H^{\mathcal{E}}$ is exactly the coherent information where $H^{\mathcal{M}}$ and $H^{\mathcal{E}}$ are the Holevo information in $\mathcal{M}$ and $\mathcal{E}$, respectively. For $\mathcal{S}$ outside of $\mathcal{M}$, $H^{\mathcal{M}}$ stays almost zero so that $C^{\mathcal{M}} \approx -H^{\mathcal{E}}$. $H^{\mathcal{E}}$ stays at maximum until starts decreasing at the τ_e point. At the scrambled point τ_s, $H^{\mathcal{E}}$ reaches its minimum and starts recovering its value until saturation at the τ_r point. With the size of $\mathcal{E}$ satisfying $\frac{N-M}{N} > \frac{1+s}{2}$, $\mathcal{E}$ obtains all the S bits after τ_r while $\mathcal{M}$ acquires no information.

One can also regard the random circuit here as the encoding operation in QEC [39–41]. Tracing $\mathcal{E}$ out would then correspond to the qubit loss error, and $C^{\mathcal{M}}$ is the number of successfully preserved logical qubits. In our result for $m < \frac{1}{2}$, the information can never be perfectly recovered from $\mathcal{M}$ as long as $\mathcal{E}$ has nonzero overlap with $\mathcal{S}$, regardless of how deep the encoding circuit is. On the other side, we can study the case when $m > \frac{1}{2}$ by exchanging $\mathcal{E}$ and $\mathcal{M}$ so that the qubits in $\mathcal{M}$ instead of $\mathcal{E}$ are lost. From $C^{\mathcal{E}} = -C^{\mathcal{M}}$, all the encoded quantum information can be recovered from $\mathcal{E}$ at the τ_r point. Our result gives the minimum and sufficient circuit depth for a perfect QEC recovery.

DPTs in Haar random circuits. To the best of our knowledge, existing methods—either analytical or numerical—are incapable of directly analyzing the information in large-scale Haar random circuit (HRC) systems. We will demonstrate that the DPT structure of information dynamics is universal across HRC and Clifford random circuits. Within the precision achievable with current methods, the critical exponent ν_0 of DPTs is also universal.

Specifically, we compare brick-wall circuits with two types of 2-qubit bricks: those generated from Haar random unitary, and those generated by uniformly sampling the Clifford group (uCRC), the latter being a unitary 2-design [42]. For an arbitrary pure initial state $|\psi_i\rangle$, the two circuits produce identical average purity of $\mathcal{M}$ [30]. In order to reduce the finite-size drifts, we fix $s = 1, m = \frac{1}{2}$, which gives a simple information dynamics containing only one DPT point τ_s.

As shown in Fig. 4(b), $h(\tau)$ of HRC for small system sizes $N \lesssim 28$ behave similarly to uCRC. We further demonstrate the universality of the critical exponent $\nu_0 = 1.25$ in the inset. For fixed δ satisfying $\delta N^{\frac{1}{\nu_0}} \ll 1$, $\partial_\tau h|_{\tau_s-\delta}^{\tau_s+\delta} \equiv \partial_\tau h(\tau_s + \delta) - \partial_\tau h(\tau_s - \delta)$ of uCRC should be proportional to $N^{\frac{1}{\nu_0}}$. This can be concluded from the collapsed $\partial_\tau h(\tau')$ in the inset of Fig. 2 with nonzero slope near $\tau' = 0$. When applying to HRC the same τ_s value from the thermodynamic limit of uCRC, the scaling behavior remains consistent $\partial_\tau h|_{\tau_s-\delta}^{\tau_s+\delta} \propto N^{\frac{1}{\nu_0}}$. More details can be found in the SM [31].

Discussion. In summary, we have studied the dynamical phase transitions in information flow with universal behavior across random unitary circuits. We identified up to four DPT points in both classical and quantum information flow: escape, accelerate, scrambled, and recover. We studied their dependence on the model configuration, uncovering the light-cone structure of information propagation. The accelerate and recover points show new stages of propagation other than ballistic and scrambling behavior. The quantum circuit ansatz we focused on already encompasses a broad range of quantum systems. The potential for similar behavior in generic systems, especially those governed by Hamiltonian dynamics, remains an area of great interest. Although we discussed the DPTs only from the information perspective, we expect similar DPT behavior in other important physical quantities. The discovery of the DPTs shall thus shed light on our understanding of generic quantum many-body dynamics.

Acknowledgment. We thank Z.-D. Liu and D. Yuan for discussions. This work was supported by the Innovation Program for Quantum Science and Technology (2021ZD0301601) and Shanghai Qi Zhi Institute. The numerical calculations in this study were carried out on the ORISE Supercomputer.

[1] R. J. Lewis-Swan, A. Safavi-Naini, A. M. Kaufman, and A. M. Rey, Dynamics of quantum information, Nat. Rev. Phys. **1**, 627 (2019).

[2] D. Harlow, Jerusalem lectures on black holes and quantum information, Rev. Mod. Phys. **88**, 015002 (2016).

[3] X.-L. Qi, Does gravity come from quantum information? Nat. Phys. **14**, 984 (2018).

[4] E. H. Lieb and D. W. Robinson, The finite group velocity of quantum spin systems, Commun. Math. Phys. **28**, 251 (1972).

[5] T. Rakovszky, S. Gopalakrishnan, S. A. Parameswaran, and F. Pollmann, Signatures of information scrambling in the dynamics of the entanglement spectrum, Phys. Rev. B **100**, 125115 (2019).

[6] P. Hayden and J. Preskill, Black holes as mirrors: Quantum information in random subsystems, J. High Energy Phys. 09 (2007) 120.

[7] Y. Sekino and L. Susskind, Fast scramblers, J. High Energy Phys. 10 (2008) 065.

[8] B. Swingle, Unscrambling the physics of out-of-time-order correlators, Nat. Phys. **14**, 988 (2018).

[9] S. H. Shenker and D. Stanford, Black holes and the butterfly effect, J. High Energ. Phys. 03 (2014) 067.

[10] T. Mori, T. N. Ikeda, E. Kaminishi, and M. Ueda, Thermalization and prethermalization in isolated quantum systems: A theoretical overview, J. Phys. B: At. Mol. Opt. Phys. **51**, 112001 (2018).

[11] D. A. Abanin, E. Altman, I. Bloch, and M. Serbyn, *Colloquium*: Many-body localization, thermalization, and entanglement, Rev. Mod. Phys. **91**, 021001 (2019).

[12] A. Nico-Katz, A. Bayat, and S. Bose, Information-theoretic memory scaling in the many-body localization transition, Phys. Rev. B **105**, 205133 (2022).

[13] C. J. Turner, A. A. Michailidis, D. A. Abanin, M. Serbyn, and Z. Papić, Weak ergodicity breaking from quantum many-body scars, Nat. Phys. **14**, 745 (2018).

[14] D. Yuan, S.-Y. Zhang, Y. Wang, L.-M. Duan, and D.-L. Deng, Quantum information scrambling in quantum many-body scarred systems, Phys. Rev. Res. **4**, 023095 (2022).

[15] A. Chandran and C. R. Laumann, Semiclassical limit for the many-body localization transition, Phys. Rev. B **92**, 024301 (2015).

[16] C. W. von Keyserlingk, T. Rakovszky, F. Pollmann, and S. L. Sondhi, Operator Hydrodynamics, OTOCs, and entanglement growth in systems without conservation laws, Phys. Rev. X **8**, 021013 (2018).

[17] T. Rakovszky, F. Pollmann, and C. W. Von Keyserlingk, Diffusive hydrodynamics of out-of-time-ordered correlators with charge conservation, Phys. Rev. X **8**, 031058 (2018).

[18] V. Khemani, A. Vishwanath, and D. A. Huse, Operator spreading and the emergence of dissipative hydrodynamics under unitary evolution with conservation laws, Phys. Rev. X **8**, 031057 (2018).

[19] P.-Y. Chang, X. Chen, S. Gopalakrishnan, and J. H. Pixley, Evolution of entanglement spectra under generic quantum dynamics, Phys. Rev. Lett. **123**, 190602 (2019).

[20] M. Heyl, Dynamical quantum phase transitions: A review, Rep. Prog. Phys. **81**, 054001 (2018).

[21] M. Heyl, A. Polkovnikov, and S. Kehrein, Dynamical quantum phase transitions in the transverse-field Ising model, Phys. Rev. Lett. **110**, 135704 (2013).

[22] B. Žunkovič, M. Heyl, M. Knap, and A. Silva, Dynamical quantum phase transitions in spin chains with long-range interactions: Merging different concepts of nonequilibrium criticality, Phys. Rev. Lett. **120**, 130601 (2018).

[23] C. Ates, B. Olmos, J. P. Garrahan, and I. Lesanovsky, Dynamical phases and intermittency of the dissipative quantum Ising model, Phys. Rev. A **85**, 043620 (2012).

[24] J. P. Garrahan and I. Lesanovsky, Thermodynamics of quantum jump trajectories, Phys. Rev. Lett. **104**, 160601 (2010).

[25] A. Deshpande, B. Fefferman, M. C. Tran, M. Foss-Feig, and A. V. Gorshkov, Dynamical phase transitions in sampling complexity, Phys. Rev. Lett. **121**, 030501 (2018).

[26] D. Gottesman, The Heisenberg representation of quantum computers (1998), in *Proceedings of the XXII International Colloquium on Group Theoretical Methods in Physics*, edited by S. P. Corney, R. Delbourgo, and P. D. Jarvis (International Press, Cambridge, 1999), pp. 32–43

[27] S. Aaronson and D. Gottesman, Improved simulation of stabilizer circuits, Phys. Rev. A **70**, 052328 (2004).

[28] D. Fattal, T. S. Cubitt, Y. Yamamoto, S. Bravyi, and I. L. Chuang, Entanglement in the stabilizer formalism, arXiv:quant-ph/0406168.

[29] A. Nahum, J. Ruhman, S. Vijay, and J. Haah, Quantum entanglement growth under random unitary dynamics, Phys. Rev. X **7**, 031016 (2017).

[30] A. Nahum, S. Vijay, and J. Haah, Operator spreading in random unitary circuits, Phys. Rev. X **8**, 021014 (2018).

[31] See Supplemental Material at http://link.aps.org/supplemental/10.1103/PhysRevResearch.5.L042043 for more details of classical information dynamics and the universality of DPTs in random quantum circuit ansatz..

[32] J.-Z. Zhuang, Y.-K. Wu, and L.-M. Duan, Phase-transition-like behavior in information retrieval of a quantum scrambled random circuit system, Phys. Rev. B **106**, 144308 (2022).

[33] H. Barnum, M. A. Nielsen, and B. Schumacher, Information transmission through a noisy quantum channel, Phys. Rev. A **57**, 4153 (1998).

[34] A. S. Holevo and V. Giovannetti, Quantum channels and their entropic characteristics, Rep. Prog. Phys. **75**, 046001 (2012).

[35] B. Schumacher and M. A. Nielsen, Quantum data processing and error correction, Phys. Rev. A **54**, 2629 (1996).

[36] F. Leditzky, D. Leung, and G. Smith, Dephrasure channel and superadditivity of coherent information, Phys. Rev. Lett. **121**, 160501 (2018).

[37] I. Devetak, The private classical capacity and quantum capacity of a quantum channel, IEEE Trans. Inform. Theory **51**, 44 (2005).

[38] K. Li, A. Winter, X. B. Zou, and G. C. Guo, Private capacity of quantum channels is not additive, Phys. Rev. Lett. **103**, 120501 (2009).

[39] W. Brown and O. Fawzi, Short random circuits define good quantum error correcting codes, in *2013 IEEE Int. Symp. Inf. Theory* (IEEE, Istanbul, Turkey, 2013), pp. 346–350.

[40] S. Choi, Y. Bao, X.-L. Qi, and E. Altman, Quantum error correction in scrambling dynamics and measurement-induced phase transition, Phys. Rev. Lett. **125**, 030505 (2020).

[41] M. J. Gullans, S. Krastanov, D. A. Huse, L. Jiang, and S. T. Flammia, Quantum coding with low-depth random circuits, Phys. Rev. X **11**, 031066 (2021).

[42] H. Zhu, Multiqubit clifford groups are unitary 3-designs, Phys. Rev. A **96**, 062336 (2017).